A Geo-Foundation Framework for Retrogressive Thaw Slump Detection Using High-resolution Remote Sensing Data

Mohammad Marjani[1], Masoud Mahdianpari[1, 2], Fariba Mohammadimanesh[3]

[1] Department of Electrical and Computer Engineering, Memorial University of Newfoundland, St. John’s, NL A1C 5S7, Canada – mmarjani@mun.ca; m.mahdianpari@mun.ca
[2] C-Core, St. John’s, NL A1B 3X5, Canada - masoud.mahdianpari@c-core.ca
[3] Canada Centre for Remote Sensing, Natural Resources Canada, 580 Booth Street, Ottawa, ON, Canada - fariba.mohammadimanesh@nrcan-rncan.gc.ca

Keywords: Retrogressive Thaw Slumps (RTS) Detection, Geo-Foundation Models, Clay Model, Deep Learning, Arctic Remote Sensing.

Abstract

Retrogressive thaw slumps (RTSs) are key indicators of permafrost degradation in Arctic regions. Yet, their detection remains challenging due to spectral similarity with surrounding terrain and the limited generalization of conventional deep learning approaches. This study presents a Geo-Foundation framework that integrates pretrained Clay embeddings with high-resolution PlanetScope multispectral imagery, spectral indices, and ArcticDEM data for RTS detection in the Northwest Territory (NWT), Canada. The proposed dual-branch architecture combines high-level geospatial representations with physically meaningful environmental features to improve segmentation performance. The model achieved an F1-score of 0.83 and a mean Intersection-over-Union (mIoU) of 0.75 on the validation dataset. Analysis of patch size indicates that intermediate spatial context provides optimal performance, while feature importance results highlight the dominant role of vegetation-sensitive spectral bands and indices. Qualitative evaluation further confirms accurate boundary delineation and spatial consistency across diverse terrain conditions. The results demonstrate that Geo-Foundation models enhance detection accuracy, reduce dependence on large labeled datasets, and improve generalization across heterogeneous Arctic landscapes. This approach provides a scalable and efficient solution for monitoring permafrost-related disturbances under a changing climate.

1. Introduction

Retrogressive thaw slumps (RTSs) are among the most evident indications of permafrost degradation across Arctic regions (Yuan et al., 2024). These thermokarst features develop when ground ice melts, leading to the retreat of steep headwalls and the formation of expanding, bowl-shaped depressions that can grow several meters annually (Nitze et al., 2018). With Arctic warming occurring at approximately twice the global rate (Rantanen et al., 2022), the frequency and spatial extent of RTSs have increased considerably in recent decades (Nitze et al., 2018). Their impacts extend beyond geomorphology, as they alter hydrological processes, remove vegetation, and release previously frozen organic carbon, potentially contributing to greenhouse gas emissions such as methane (Marjani, Mahdianpari, Varon, et al., 2025; Mohammadimanesh et al., 2025). In addition, RTS activity threatens infrastructure and affects land use in northern communities (Alizadeh et al., 2025). As a result, RTSs serve as critical indicators of permafrost stability and the effects of climate change.

Despite their importance, large-scale detection and monitoring of RTSs remain challenging. These features are often small, spatially dispersed, and located in remote areas with limited accessibility (Huang et al., 2022). Their rapid evolution introduces temporal variability, while differences in geological and environmental conditions lead to substantial heterogeneity in their spectral and morphological characteristics (Yang et al., 2023). These factors complicate consistent identification across regions.

Remote sensing has become a primary tool for RTS monitoring, providing repeated observations over extensive and inaccessible Arctic landscapes. Optical sensors, including Landsat and Sentinel-2, measure surface changes related to vegetation loss, exposed soil, and water accumulation (Igwe et al., 2026; Marjani et al., 2025). However, traditional mapping approaches often rely on manual interpretation or simple threshold-based methods, which are labor-intensive and struggle to generalize due to spectral confusion with other land surface features (Mahdianpari et al., 2026).

Deep learning methods have improved automated RTS detection by capturing complex spatial patterns in remote sensing data. Architectures such as UNet, DeepLabV3, and ResNet-based models have demonstrated notable performance gains (Huang et al., 2022; Nitze et al., 2021; Wu et al., 2025). For instance, intersection over union (IoU) values have increased from approximately 0.58 to 0.80 across different studies. Nevertheless, these approaches typically require large labeled datasets, which remain scarce in Arctic environments, limiting their scalability and transferability (Nitze et al., 2025).

Recent advances in foundation models have introduced a new paradigm in geospatial analysis. These models are pre-trained on large-scale Earth observation (EO) datasets and learn transferable representations that can be adapted to various tasks with minimal labeled data (Janowicz et al., 2025). Among these, the Clay model captures spectral, spatial, and contextual information from diverse environments, providing embeddings that enhance feature representation and improve generalization across regions.

In this study, we present a Geo-Foundation-based framework that integrates Clay embeddings with PlanetScope multispectral imagery, spectral indices, and ArcticDEM data for RTS detection. The proposed approach aims to (i) evaluate the contribution of pretrained geospatial embeddings to detection performance and (ii) assess the role of multi-source input features through systematic analysis. This framework provides a scalable and data-efficient solution for monitoring permafrost degradation across Arctic landscapes.

2. Material and Method

2.1 Study Area and Reference Data

The study focuses on a permafrost-dominated region in the Northwest Territories (NWT), Canada, which represents a highly dynamic Arctic environment where RTSs are widespread due to interacting climatic, geomorphological, and permafrost conditions (Segal et al., 2016). The landscape reflects a strong glacial legacy, consisting of ice-rich moraines, glaciolacustrine deposits, and upland terrains that create favorable slope conditions for slump development. Permafrost conditions in this region range from continuous to discontinuous, with high ground ice content that plays a key role in RTS initiation.

Ground reference data were compiled through a combination of field observations, high-resolution imagery, and expert interpretation. RTS polygons were delineated and split into training and validation subsets at an 80/20 ratio to support model development and evaluation (see Figure 1).

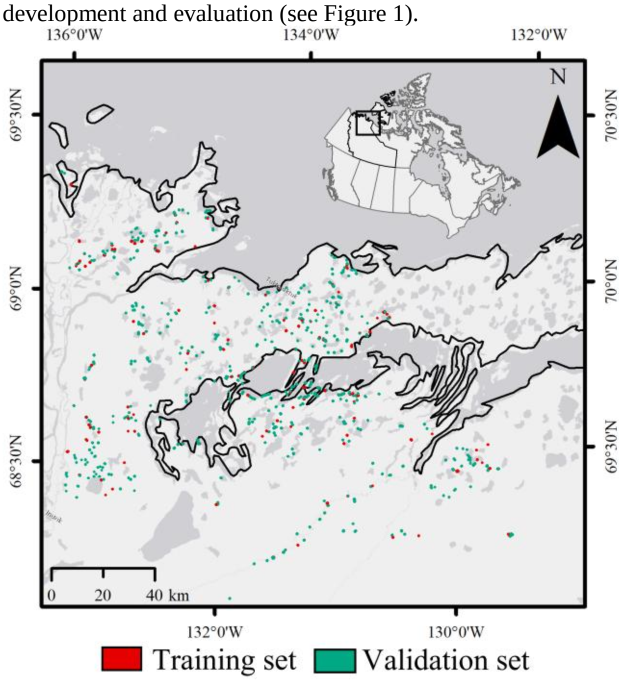

Figure 1. The extent of the study area in NWT.

2.2 Satellite Data

High-resolution multispectral imagery from PlanetScope was used as the primary data source due to its ability to represent fine-scale geomorphic features. The PlanetScope constellation provides imagery at approximately 3 m spatial resolution with a near-daily revisit frequency, enabling the observation of small, rapidly evolving land surface changes.

Eight spectral bands were used in this study, including Coastal, Blue, Green I, Green, Yellow, Red, Red Edge, and Near-Infrared (NIR). These bands represent variations in vegetation condition, soil exposure, and moisture, which are essential for identifying RTS features. To maintain data quality, imagery acquired between 6 and 8 August 2024 with less than 5% cloud cover was selected, corresponding to peak summer conditions in the study region.

2.3 Derived and Ancillary Data

To better model environmental processes associated with RTSs, additional data layers were integrated with the multispectral imagery. Spectral indices derived from PlanetScope bands were used to highlight key surface characteristics. Vegetation-related indices, including the Normalized Difference Vegetation Index (NDVI), Enhanced Vegetation Index (EVI), and Normalized Difference Red Edge Index (NDRE), indicate vegetation degradation and stress near slump boundaries. In contrast, the Normalized Difference Water Index (NDWI) reflects water accumulation within slump floors. Indices such as the Redness Index (RI), Excess Green Index (ExG), and the Brightness Index enhance the detection of exposed soil and ice, improving the distinction between disturbed and undisturbed areas.

In addition, topographic information from ArcticDEM was incorporated to provide terrain context. ArcticDEM is a high-resolution elevation dataset derived from stereo satellite imagery (Dai et al., 2024) that provides a detailed representation of Arctic surface morphology at approximately 2 m spatial resolution. In this study, the data were resampled to 3 m to align with PlanetScope imagery. Including elevation enables the model to account for terrain-related factors influencing RTS development, such as slope, relief, and geomorphic setting.

2.4 Data Preparation

Training samples were generated by integrating PlanetScope imagery, derived datasets (spectral indices and ArcticDEM), and digitized RTS polygons into a unified patch-based framework, as shown in Figure 2. The preparation process followed a structured pipeline that included patch generation, spatial filtering, and label construction. In the first step, all input layers were segmented into 64 × 64-pixel tiles with 50% overlap. Each patch was then evaluated based on its spatial overlap with RTS polygons. Let A denote the intersection area between a patch and the RTS polygons, and let A′ represent 10% of the patch area. Only patches satisfying A>A′ were retained, which guaranteed that each selected sample contained a meaningful representation of RTS features and limited the inclusion of background-dominated regions.

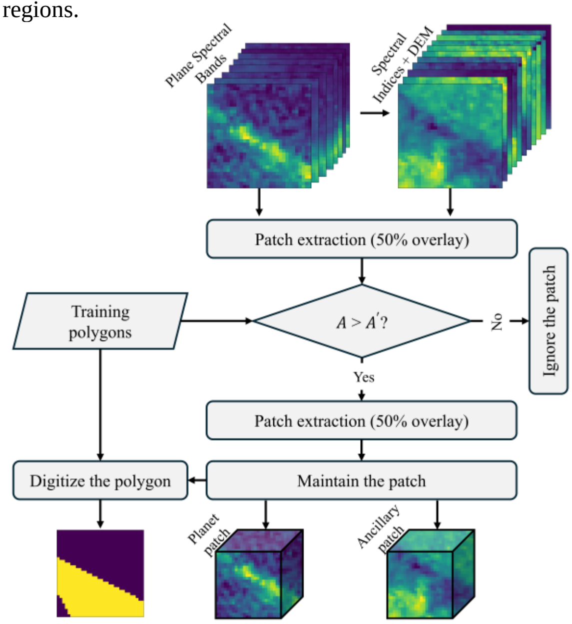

Figure 2. Data preparation workflow used in this study.

For the retained samples, corresponding labels were generated by rasterizing the RTS polygons into binary masks, assigning RTS pixels a value of 1 and all other pixels a value of 0. During this step, geospatial metadata, including coordinate reference system (CRS), spatial resolution, and affine transformation, were preserved to maintain precise alignment between imagery and labels. All ancillary datasets were resampled and aligned to the same grid as the PlanetScope imagery to achieve full spatial consistency across inputs.

The final dataset consisted of two complementary components: (i) multispectral image patches used as input to the Geo-Foundation model for embedding extraction, and (ii) aligned ancillary patches combined with these embeddings during model training.

2.5 Geo-Foundation Models and Clay

Geo-foundation models extend conventional deep learning approaches using large-scale pretraining on EO data. Unlike standard models trained on limited labeled datasets, these models learn transferable representations from multispectral imagery, temporal sequences, and geospatial metadata through self-supervised strategies such as masked autoencoding (Jakubik et al., 2023). This capability allows them to generalize across different regions and environmental conditions with reduced dependence on annotated data.

Among these models, the Clay Geo-Foundation model provides a comprehensive framework for extracting geospatial representations from multi-source EO data. Clay is trained on large-scale satellite archives and encodes spectral, spatial, and contextual information into high-dimensional embeddings. These embeddings indicate relationships between surface properties, sensor characteristics, and environmental conditions, making them highly suitable for geomorphological applications. In addition to multispectral inputs, Clay incorporates auxiliary metadata such as geographic coordinates, acquisition time, ground sampling distance (GSD), and spectral wavelengths, which further enrich the learned representations. The model follows a transformer-based architecture (Marjani et al., 2025; Mohammadimanesh et al., 2026), where input patches are encoded into latent features that preserve semantic information while reducing spatial resolution. This design enables efficient processing of large-scale imagery while maintaining meaningful contextual information. An overview of Clay model is shown in Figure 3.

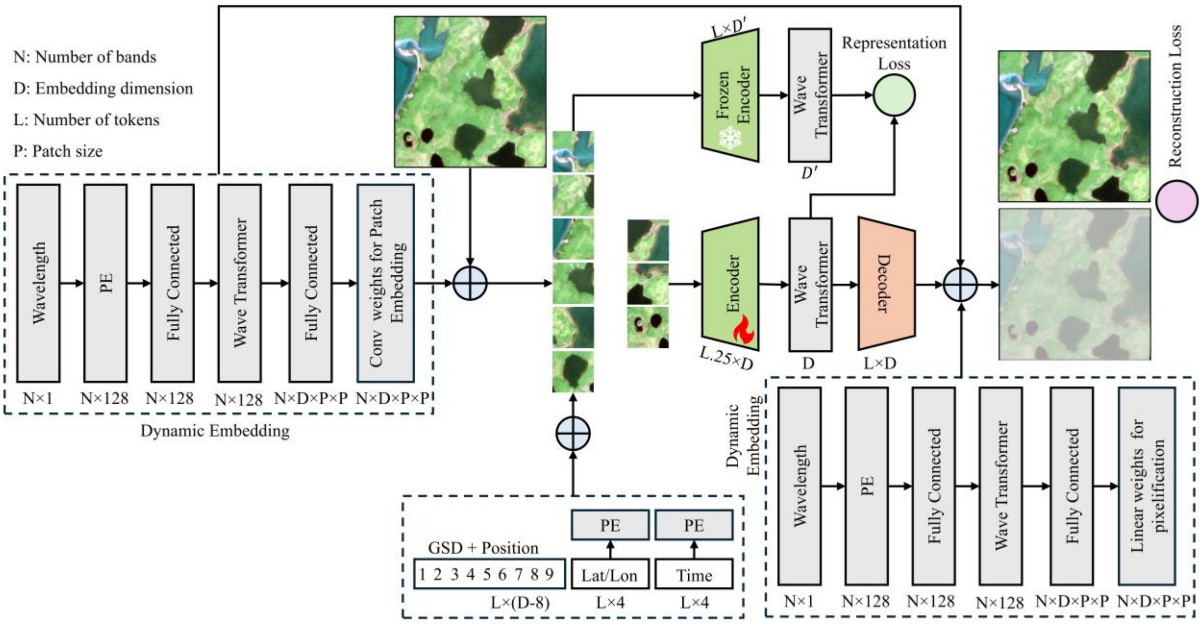

Figure 3. An overview of the Clay Geo-Foundation model.

A key advantage of Clay is its ability to enhance feature separability among subtle land surface classes. In the context of RTS detection, this capability is particularly important due to the spectral similarity between disturbed and undisturbed permafrost surfaces. By leveraging pretrained embeddings, Clay reduces the reliance on extensive labeled datasets and improves model transferability across heterogeneous Arctic landscapes.

2.6 Geo-Foundation Training

To exploit the strengths of the Clay model, a hybrid training framework was designed that integrates pretrained embeddings with high-resolution ancillary data. PlanetScope patches, together with associated metadata, were first processed through the non-trainable Clay encoder to generate compact, high-dimensional feature representations. These embeddings encode semantic and contextual information derived from large-scale EO pretraining.

In parallel, ancillary datasets, including spectral indices and elevation data, were processed through a trainable UNet encoder (Marjani et al., 2026) to extract detailed environmental features related to vegetation condition, soil exposure, moisture, and terrain morphology. The outputs from both branches were fused in latent space, followed by a channel-attention mechanism (Marjani et al., 2024) that prioritizes the most informative features. The combined representation was then decoded using a UNet decoder to produce pixel-level RTS predictions.

This dual-stream design enables the model to benefit from both generalized representations learned by Clay and fine-scale information provided by ancillary data. As a result, the framework improves the detection of subtle RTS boundaries and enhances robustness across varying terrain and environmental conditions. This dual architecture is illustrated in Figure 4.

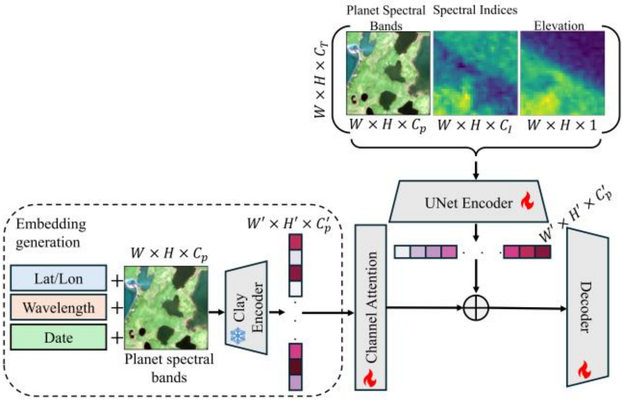

Figure 4. Training workflow that integrates PlanetScope spectral patches with derived spectral indices and elevation data in a dual-stream architecture.

3. Results

3.1 Optimal Patch Size

To evaluate the patch size effect, four patch sizes (32×32, 64×64, 128×128, and 256×256) were tested using the proposed framework that integrates PlanetScope imagery with Clay embeddings. Table 1 summarizes the mean intersection over union (mIoU) values obtained on the validation dataset. The results indicate that model performance is highly sensitive to patch size. The best performance was achieved with a patch size of 64×64, reaching an mIoU of 0.75. This result suggests that moderate-sized patches provide an optimal balance between extracting local RTS characteristics and preserving sufficient contextual information.

At smaller patch sizes (32×32), the model achieved competitive performance (mIoU = 0.65), indicating that integrating Clay embeddings can partially compensate for limited spatial context by providing semantically rich representations. However, increasing the patch size beyond 64×64 led to a decline in performance. Specifically, mIoU decreased to 0.71 for 128×128 and further dropped to 0.56 for 256×256 patches. This reduction can be attributed to the inclusion of excessive background information, which dilutes the distinctive spectral and geomorphological signatures of RTSs.

Table 1. mIoU values for different patch sizes using the proposed framework.

Patch size	mIoU
32×32	0.65
64×64	0.75
128×128	0.71
256×256	0.56

3.2 RTS Detection Results

The performance of the proposed framework on the training and validation datasets is presented in Figure 5. The results demonstrate strong and consistent performance across all evaluation metrics. On the validation set, the model achieved a precision of 0.82, a recall of 0.85, an F1-score of 0.83, and an mIoU of 0.75, indicating reliable detection of RTS features with a good balance between omission and commission errors. The relatively high recall suggests that most RTS pixels are correctly identified, while the precision indicates that false detections remain limited.

Performance on the training set is slightly higher, with precision = 0.87, recall = 0.93, F1-score = 0.90, and mIoU = 0.79. The close agreement between the training and validation results indicates stable learning behavior and good generalization, with no significant evidence of overfitting.

The F1-score values in both datasets highlight a balanced trade-off between precision and recall, while the mIoU scores confirm accurate spatial delineation of RTS boundaries. These results show that integrating Clay embeddings with multispectral and ancillary data enables the model to capture the contextual and fine-scale characteristics of RTS features accurately.

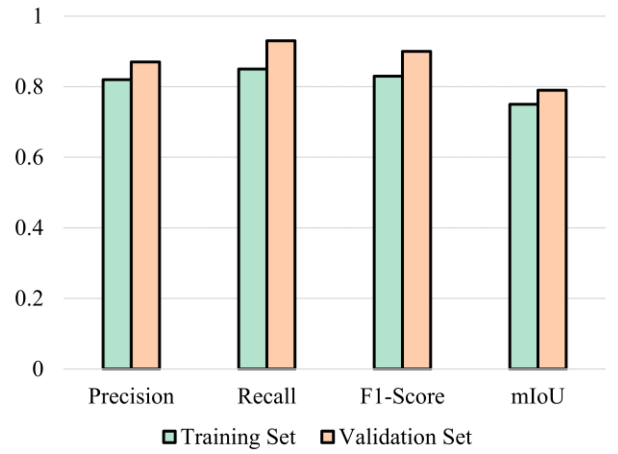

Figure 5. Performance comparison of the proposed RTS detection model on training and validation datasets.

In addition to the quantitative evaluation, Figure 6 presents representative qualitative results of RTS detection, illustrating the model’s ability to delineate slump features across different landscape conditions accurately. The figure combines multiple data layers, including PlanetScope RGB imagery, ArcticDEM elevation, and statistical summaries (mean and standard deviation) of the Clay embeddings, providing an understanding of how spatial, spectral, and learned representations contribute to detection performance. Corresponding ground-truth labels, model predictions, and pixel-level confusion matrix maps are also shown for comparison.

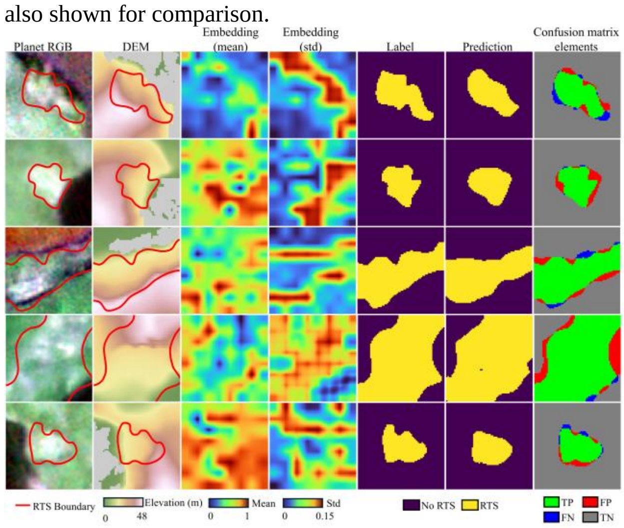

https://doi.org/10.5194/isprs-archives-XLIX-B1-2026-639-2026

Figure 6. Qualitative RTS detection results showing PlanetScope RGB imagery, ArcticDEM elevation, Clay embedding statistics (mean and standard deviation), ground-truth labels, model predictions, and pixel-wise confusion matrix elements (TP, FP, FN, TN).

The results demonstrate strong agreement between predicted outputs and reference labels. True positive (TP) regions closely follow the RTS boundaries, indicating that the model extracts the extent and morphology of slump features. False positives (FPs) are generally limited and occur mainly in transitional areas, such as terrain edges or regions affected by surface moisture and illumination variability. False negatives (FNs) are rare and primarily occur along complex or irregular headwall boundaries, where abrupt changes in topography and spectral properties make classification more difficult.

3.3 Feature Importance

Feature importance analysis was conducted to assess how individual inputs contribute to RTS detection performance. This step provides an understanding of the model's decision-making process by linking predictions to physically meaningful surface characteristics, rather than treating the model as an opaque system. Such interpretation is particularly important in EO applications, where variables such as vegetation condition, soil exposure, and terrain properties are directly associated with RTS dynamics.

An occlusion-based sensitivity analysis was employed to quantify the contribution of each input layer. The model was first evaluated using the full set of 19 inputs, including PlanetScope spectral bands, derived indices, and elevation data, to establish a baseline mIoU. Subsequently, each feature was removed independently by setting its values to zero, and the model was re-evaluated. The decrease in mIoU relative to the baseline was used as a measure of feature importance, with larger reductions indicating a stronger influence on model performance.

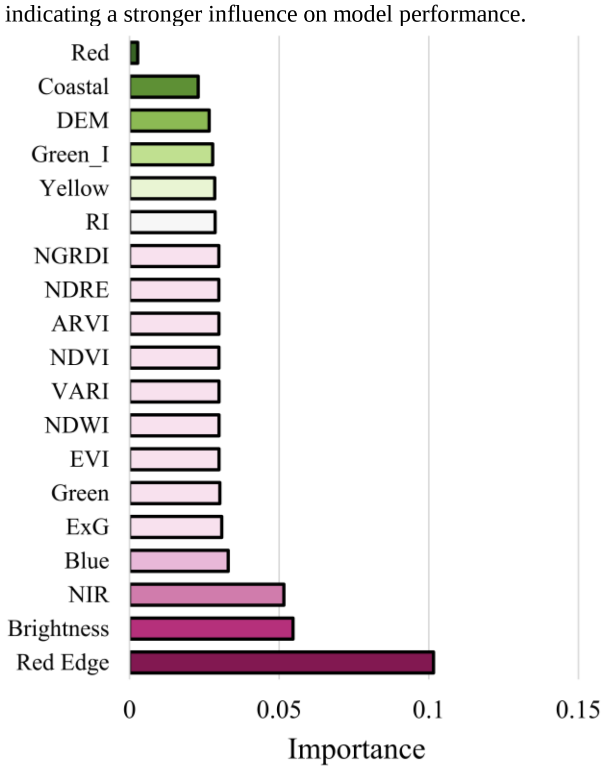

Figure 7. Relative importance of input features, including PlanetScope spectral bands, spectral indices, and ArcticDEM elevation, measured by the decrease in mIoU after feature occlusion. Larger values correspond to stronger influence on model predictions.

The results, illustrated in Figure 7, reveal that the Red Edge band has the highest impact (importance ≈ 0.12), highlighting its sensitivity to vegetation stress and spectral transitions commonly observed near active slump boundaries. The Brightness index and Near-Infrared (NIR) band also contribute significantly (≈ 0.06), emphasizing the role of surface reflectance and vegetation characteristics in distinguishing disturbed from undisturbed areas. Several vegetation and moisture-related indices, including ExG, NDVI, EVI, and NDWI, show moderate importance (≈ 0.03), indicating their relevance in capturing degradation and moisture patterns associated with RTS activity.

In contrast, elevation derived from ArcticDEM contributes less (≈ 0.027), suggesting that topographic information provides complementary but less dominant cues for classification. The Red and Coastal bands demonstrate minimal influence (≈ 0.002–0.02), likely due to redundancy with more informative spectral channels such as NIR and Red Edge.

4. Discussion

The results indicate that RTS detection is strongly controlled by spatial context and surface characteristics. The patch-size analysis shows that intermediate spatial windows achieve the highest accuracy, indicating that effective detection requires a balance between fine-scale detail and broader geomorphological context. Smaller patches emphasize local features but lack sufficient surrounding information, while larger patches introduce redundant background that reduces class separability. Similar scale-dependent behavior has been reported in previous geomorphological mapping studies, where both object size and contextual information influence detection accuracy (Huang et al., 2020; Wu et al., 2025).

The feature importance analysis further demonstrates that vegetation-sensitive spectral bands and indices play a dominant role in RTS detection. The strong contribution of the Red Edge and NIR bands highlights their sensitivity to vegetation stress and surface disturbance, which are key indicators of thaw-related processes (Gooseff et al., 2009; Huang et al., 2020). In addition, indices such as NDVI, EVI, and NDWI capture vegetation degradation and moisture dynamics associated with active slumps, consistent with previous findings on thermokarst evolution and ecological response (Turetsky et al., 2020; Yin et al., 2017). In contrast, elevation derived from ArcticDEM shows a lower contribution, indicating that topographic variables provide complementary but less direct information for RTS delineation in high-resolution optical imagery (Lewkowicz & Way, 2019).

A key outcome of this study is the demonstrated effectiveness of integrating Geo-Foundation embeddings into the detection framework. The Clay model encodes spatial–spectral relationships learned from large-scale EO datasets, enabling it to extract complex patterns that are difficult to represent with conventional inputs alone (Janowicz et al., 2025; Xiao et al., 2025). This capability improves the separation between disturbed and undisturbed terrain, particularly in areas with limited spectral contrast. As a result, the model produces more coherent predictions and more accurate boundary delineation, which aligns with recent advances in foundation models for geospatial analysis (Jakubik et al., 2023).

Compared to traditional deep learning approaches, which often require extensive labeled datasets and exhibit limited transferability, the proposed framework benefits from pretrained representations that enhance generalization across heterogeneous environments. Previous RTS mapping studies based on CNN architectures have reported challenges related to domain variability, spectral confusion, and limited training data (Huang et al., 2022; Udawalpola et al., 2022; Yang et al., 2023). By leveraging foundation model embeddings, the proposed approach reduces sensitivity to these factors and improves robustness under varying environmental conditions.

Despite these advantages, several limitations remain. The reliance on optical imagery limits performance under cloud cover and low illumination, which are common in Arctic regions. In addition, the current framework integrates ancillary data outside the foundation model, indicating that cross-modal fusion is not fully optimized. The computational cost of generating high-dimensional embeddings also poses challenges for large-scale or near-real-time applications. Future work should explore integrating multi-sensor data, such as SAR imagery, and developing more efficient embedding representations to improve scalability and operational applicability.

5. Conclusion

This study presented a Geo-Foundation framework for automated RTS detection in the NWT using PlanetScope imagery, derived spectral indices, and ArcticDEM data. By integrating pretrained Clay embeddings within a dual-branch architecture, the proposed approach effectively combines high-level contextual representations with physically meaningful environmental features. The results demonstrated strong performance, achieving an F1-score of 0.83 and an mIoU of 0.75, which confirms the effectiveness of leveraging foundation models for improving detection accuracy in complex Arctic environments.

The analysis showed that vegetation-related spectral features play a dominant role in RTS identification, while elevation contributes complementary information. The integration of Clay embeddings enhanced feature representation and improved the model's ability to distinguish subtle differences between disturbed and stable terrain. In addition, the framework showed consistent performance across varying spatial conditions, highlighting its robustness for mapping heterogeneous permafrost landscapes.

The findings suggest that Geo-Foundation models provide a scalable and data-efficient solution for RTS detection, reducing reliance on large labeled datasets and improving generalization across regions. However, challenges remain, including the reliance on optical data, limited integration of multi-sensor inputs, and the computational cost associated with embedding generation. Future research should explore multimodal data fusion, including SAR, and develop more efficient architectures to support large-scale and operational applications.

References

Alizadeh, N., Mahdianpari, M., Hemmati, E., & Marjani, M. (2025). FusionFireNet: A CNN-LSTM model for short-term wildfire hotspot prediction utilizing spatio-temporal datasets. *Remote Sensing Applications: Society and Environment*, *37*, 101436.

Dai, C., Howat, I. M., van der Sluijs, J., Liljedahl, A. K., Higman, B., Freymueller, J. T., Jones, M. K. W., Kokelj, S. V., Boike, J., & Walker, B. (2024). Applications of ArcticDEM for measuring volcanic dynamics, landslides, retrogressive thaw slumps, snowdrifts, and vegetation heights. *Science of Remote Sensing*, *9*, 100130.

Gooseff, M. N., Balser, A., Bowden, W. B., & Jones, J. B. (2009). Effects of Hillslope Thermokarst in Northern Alaska. *Eos, Transactions American Geophysical Union*, *90*(4), 29–30. https://doi.org/10.1029/2009EO040001

Huang, L., Lantz, T. C., Fraser, R. H., Tiampo, K. F., Willis, M. J., & Schaefer, K. (2022). Accuracy, Efficiency, and Transferability of a Deep Learning Model for Mapping Retrogressive Thaw Slumps across the Canadian Arctic. *Remote Sensing*, *14*(12), Article 12. https://doi.org/10.3390/rs14122747

Huang, L., Luo, J., Lin, Z., Niu, F., & Liu, L. (2020). Using deep learning to map retrogressive thaw slumps in the Beiluhe region (Tibetan Plateau) from CubeSat images. *Remote Sensing of Environment*, *237*, 111534. https://doi.org/10.1016/j.rse.2019.111534

Igwe, V., Salehi, B., Marjani, M., Farhadi, N., & Mahdianpari, M. (2026). Cost-effective statewide wetland inventory update using weakly supervised deep learning: A case study in Minnesota, USA. *Remote Sensing Applications: Society and Environment*, 101871.

Jakubik, J., Roy, S., Phillips, C. E., Fraccaro, P., Godwin, D., Zadrozny, B., Szwarcman, D., Gomes, C., Nyirjesy, G., Edwards, B., Kimura, D., Simumba, N., Chu, L., Mukkavilli, S. K., Lambhate, D., Das, K., Bangalore, R., Oliveira, D., Muszynski, M., … Ramachandran, R. (2023). *Foundation Models for Generalist Geospatial Artificial Intelligence* (arXiv:2310.18660). arXiv. https://doi.org/10.48550/arXiv.2310.18660

Janowicz, K., Mai, G., Huang, W., Zhu, R., Lao, N., & Cai, L. (2025). GeoFM: How will geo-foundation models reshape spatial data science and GeoAI? *International Journal of Geographical Information Science*, *39*(9), 1849–1865. https://doi.org/10.1080/13658816.2025.2543038

Lewkowicz, A. G., & Way, R. G. (2019). Extremes of summer climate trigger thousands of thermokarst landslides in a High Arctic environment. *Nature Communications*, *10*(1), 1329.

Mahdianpari, M., Sonnentag, O., Mohammadimanesh, F., Radman, A., Marjani, M., Morse, P., Marsh, P., Lavoie, M., Risk, D., & Wu, J. (2026). State of the Art in Monitoring Methane Emissions from Arctic–boreal Wetlands and Lakes. *Remote Sensing*. https://www.mdpi.com/2072-4292/18/6/926

Marjani, M., Mahdianpari, M., Gill, E. W., & Mohammadimanesh, F. (2025). A Dual-Branch Deep Learning Framework for Wetland Mapping Using Sentinel-1 and Sentinel-2. *2025 IEEE 20th International Symposium on Antenna Technology and Applied Electromagnetics (ANTEM)*, 246–249. https://ieeexplore.ieee.org/abstract/document/11114179/

Marjani, M., Mahdianpari, M., Gill., E. W., & Mohammadimanesh, F. (2025). Explainable AI for Wetland Mapping Using High-Resolution Remote Sensing Data. *IGARSS 2025 - 2025 IEEE International Geoscience and Remote Sensing Symposium*, 3841–3844.

https://doi.org/10.1109/IGARSS55030.2025.11243021

Marjani, M., Mahdianpari, M., Mohammadimanesh, F., & Gill, E. W. (2024). CVTNet: A fusion of convolutional neural networks and vision transformer for wetland mapping using Sentinel-1 and Sentinel-2 satellite data. *Remote Sensing*, *16*(13), 2427.

Marjani, M., Mahdianpari, M., Varon, D. J., & Mohammadimanesh, F. (2025). The integration of vision transformers and SAM for automated methane super-emitter detection using TROPOMI data. *Journal of Environmental Management*, *393*, 127034.

Marjani, M., Mohammadimanesh, F., & Mahdianpari, M. (2026). ABNextFire: A Multi-Source Deep Learning Based Dataset for Wildfire Spread Prediction. *IEEE Journal of Selected Topics in Applied Earth Observations and Remote Sensing*, 1–21. https://doi.org/10.1109/JSTARS.2026.3677699

Mohammadimanesh, F., Mahdianpari, M., Radman, A., Varon, D., Hemati, M., & Marjani, M. (2025). Advancements in satellite-based methane point source monitoring: A systematic review. *ISPRS Journal of Photogrammetry and Remote Sensing*, *224*, 94–112. https://doi.org/10.1016/j.isprsjprs.2025.03.020

Mohammadimanesh, F., Marjani, M., & Mahdianpari, M. (2026). HiResNet: A Low-to-High Deep Learning Framework for Updating Large-Scale Land-Cover Inventory. *IEEE Transactions on Geoscience and Remote Sensing*, 1–1. https://doi.org/10.1109/TGRS.2026.3676677

Nitze, I., Grosse, G., Jones, B. M., Romanovsky, V. E., & Boike, J. (2018). Remote sensing quantifies widespread abundance of permafrost region disturbances across the Arctic and Subarctic. *Nature Communications*, *9*(1), 5423.

Nitze, I., Heidler, K., Barth, S., & Grosse, G. (2021). Developing and Testing a Deep Learning Approach for Mapping Retrogressive Thaw Slumps. *Remote Sensing*, *13*(21), 4294. https://doi.org/10.3390/rs13214294

Nitze, I., Heidler, K., Nesterova, N., Küpper, J., Schütt, E., Hölzer, T., Barth, S., Lara, M. J., Liljedahl, A. K., & Grosse, G. (2025). DARTS: Multi-year database of AI-detected retrogressive thaw slumps in the circum-arctic permafrost region. *Scientific Data*, *12*(1), 1512.

Rantanen, M., Karpechko, A. Y., Lipponen, A., Nordling, K., Hyvärinen, O., Ruosteenoja, K., Vihma, T., & Laaksonen, A. (2022). The Arctic has warmed nearly four times faster than the globe since 1979. *Communications Earth & Environment*, *3*(1), 168.

Segal, R. A., Lantz, T. C., & Kokelj, S. V. (2016). Acceleration of thaw slump activity in glaciated landscapes of the Western Canadian Arctic. *Environmental Research Letters*, *11*(3), 034025.

Turetsky, M. R., Abbott, B. W., Jones, M. C., Anthony, K. W., Olefeldt, D., Schuur, E. A., Grosse, G., Kuhry, P., Hugelius, G., & Koven, C. (2020). Carbon release through abrupt permafrost thaw. *Nature Geoscience*, *13*(2), 138–143.

Udawalpola, M. R., Witharana, C., Hasan, A., Liljedahl, A., Ward Jones, M., & Jones, B. (2022). Automated recognition of permafrost disturbances using high-spatial resolution satellite imagery and deep learning models. *The International Archives of the Photogrammetry, Remote Sensing and Spatial Information Sciences*, *46*. https://par.nsf.gov/biblio/10468986

Wu, F., Jiang, C., Wang, C., Zou, L., Li, T., Guan, S., & Tang, Y. (2025). Retrogressive thaw slumps recognition and occurrence analysis using deep learning with satellite remote sensing in the central Qinghai-Tibet Plateau. *Geomorphology*, *471*, 109581. https://doi.org/10.1016/j.geomorph.2024.109581

Xiao, A., Xuan, W., Wang, J., Huang, J., Tao, D., Lu, S., & Yokoya, N. (2025). Foundation models for remote sensing and earth observation: A survey. *IEEE Geoscience and Remote Sensing Magazine*. https://ieeexplore.ieee.org/abstract/document/11097335/

Yang, Y., Rogers, B. M., Fiske, G., Watts, J., Potter, S., Windholz, T., Mullen, A., Nitze, I., & Natali, S. M. (2023). Mapping retrogressive thaw slumps using deep neural networks. *Remote Sensing of Environment*, *288*, 113495. https://doi.org/10.1016/j.rse.2023.113495

Yin, G., Niu, F., Lin, Z., Luo, J., & Liu, M. (2017). Effects of local factors and climate on permafrost conditions and distribution in Beiluhe basin, Qinghai-Tibet Plateau, China. *Science of the Total Environment*, *581*, 472–485.

Yuan, Y., Zhou, G., Su, Z., Liu, Z., Sun, W., Meng, X., Wen, J., & Wu, Z. (2024). A Lightweight and Enhanced Semantic Segmentation Network for Mapping of Retrogressive Thaw Slumps from Sentinel-2 Images. *IGARSS 2024-2024 IEEE International Geoscience and Remote Sensing Symposium*, 130–133. https://ieeexplore.ieee.org/abstract/document/10641527/